Journal of Nuclear Materials 406 (2010) 323–329

Contents lists available at ScienceDirect

Journal of Nuclear Materials

journal homepage: www.elsevier.com/locate/jnucmat

First principles study of intrinsic defects in hexagonal tungsten carbide

Xiang-Shan Kong [a], Yu-Wei You [a], J.H. Xia [a], C.S. Liu [a,*], Q.F. Fang [a], G.-N. Luo [b], Qun-Ying Huang [b]

[a] Key Laboratory of Materials Physics, Institute of Solid State Physics, Chinese Academy of Sciences, P.O. Box 1129, Hefei 230031, PR China
[b] Institute of Plasma Physics, Chinese Academy of Sciences, Hefei 230031, PR China

ARTICLE INFO

Article history:
Received 14 May 2010
Accepted 2 September 2010

ABSTRACT

The characteristics of intrinsic defects are important for the understanding of self-diffusion processes, mechanical strength, brittleness, and plasticity of tungsten carbide, which are present in the divertor of fusion reactors. Here, we use first-principles calculations to investigate the stability of point defects and their complexes in tungsten carbide. Our results confirm that the defect formation energies of carbon are much lower than that of tungsten and reveal the carbon vacancy to be the dominant defect in tungsten carbide. The C—C dimer configuration along the dense ***a*** direction is the most stable configuration of carbon interstitial defect. The results of carbon defect diffusion show that the carbon vacancy stay for a wide range of temperature because of extremely high diffusion barriers, while carbon interstitial migration is activated at lower temperatures for its considerably lower activation energy. Both of them prefer to diffusion in carbon basal plane.

1. Introduction

The International Thermonuclear Experimental Reactor (ITER) is designed with a beryllium first wall, tungsten armor in the baffle and divertor regions, and carbon strike point plates [1–3]. Due to high particle and heat loads, the wall material will be eroded and migrate as plasma impurity to other parts. This leads to the formation of mixed material layers on the wall surface. Previous studies have indicated that a tungsten carbide (WC) layer could be formed during the bombardment of tungsten by carbon impurity [4–6]. In addition, WC is of practical interest for engineering application due to its high melting points, extreme hardness, good corrosion and temperature stability [7–9].

WC is stable in a hexagonal structure, which consists of alternating simple hexagonal layers of carbon and layers of tungsten. Extensive theoretical studies have been performed to understand the electronic structure and the origin of properties of WC such as hardness, bulk module and stability [10–13]. While, much less information is available for the intrinsic defects of WC, which are important for the understanding of self-diffusion processes, mechanical strength, brittleness, and plasticity. This may be related to the relatively low concentration of atomic defects on the tungsten and carbon sublattices. However, the defect concentration is increased greatly in WC under high-energy particles irradiation.

Remple et al. [14] firstly identified carbon and tungsten vacancies by positron annihilation method and found the former to be formed preferentially. Then, Ivanovskii et al. [15,16] studied the effect of tungsten and carbon vacancies on the WC band structure using first-principles full-potential linear muffin-tin orbital (FPLMTO) approach. *A vacancy peak* of the DOS was observed and the formation energies of vacancies were calculated, i.e., 0.13 Ry (1.77 eV) and 0.20 Ry (2.72 eV) for carbon and tungsten vacancy, respectively. Thereafter, Juslin et al. [17] and Björkas et al. [18] employed the molecular dynamic method to investigate the intrinsic defects in WC. They also obtained the formation energy of tungsten/carbon vacancy and interstitial: about 12 eV for tungsten interstitial and 3 eV for tungsten vacancy; 2.7 and 0.5 eV for carbon interstitial and vacancy, respectively. The comparison of above-mentioned results clearly indicate that there exists a big difference in the formation energy of carbon vacancy by different authors. Recently, Björkas et al. [18] studied the initial state of irradiation damage in WC using molecular dynamics computer simulations. They found that an in-cascade defect recombination effect, related to the large difference in the defect formation energy between tungsten and carbon, leads to large asymmetry between tungsten and carbon defects in irradiated WC. Even though certain details of the electronic structure and formation energy of intrinsic defects in WC have been addressed by aforementioned studies, several questions on the structure and stability of native point defects of WC remain open, including the atomic-scale mechanisms of defect migration.

In this paper we employ first-principles calculations to study the six possible types of native point defects of WC: carbon (V_C) and tungsten (V_W) vacancies, carbon (C_W) and tungsten (W_C) antisites, and carbon (I_C) and tungsten (I_W) interstitials. The formation energies of point defects are obtained, and the most stable interstitial configurations are identified by relaxing various possible

* Corresponding author. Tel.: +86 551 5591062.
E-mail address: csliu@issp.ac.cn (C.S. Liu).

0022-3115/$ - see front matter © 2010 Elsevier B.V. All rights reserved.
doi:10.1016/j.jnucmat.2010.09.002

configurations of carbon and tungsten interstitial structure. Besides, we investigate the atomic-scale mechanisms of carbon defect migration by the nudged elastic band method. Our calculations will provide a useful reference for further exploration of the defect properties in WC.

2. Computation method

The present calculations have been performed within density functional theory as implemented in the Vienna *ab initio* simulation package (VASP) [19,20]. The interaction between ions and electrons is described by the projector augmented wave potential (PAW) method [21,22]. Exchange and correlation functions are taken in a form proposed by Perdew and Wang (PW91) [23] within the generalized gradient approximation (GGA). The supercell approach with periodic boundary conditions is used to study defect properties, as well as defect-free system. The perfect supercell contains 128 atoms (64 carbon atoms and 64 tungsten atoms) with $4 \times 4 \times 4$ unit cells. The relaxations of atomic position and optimizations of the shape and size of the supecell are performed with the plane-wave basis sets with the energy cutoff of 500 eV throughout this work, which was checked for convergence to be within 0.001 eV per atom in the perfect supercell. Ion relaxations are performed using the standard conjugated-gradient algorithms as implemented in the VASP code. During the relaxations, the Brillouin zone (BZ) integrations is achieved using a Methfessel–Pazton smearing of sigma = 0.39 eV. BZ sampling was performed using the Monkhorst–Pack scheme [24], with a $3 \times 3 \times 3$ k-point mesh centered on the Gamma point. The structural optimization is truncated when the forces converge to less than 0.1 eV/nm.

The ground-state properties of WC, including equilibrium lattice parameters and bulk cohesive energy, have been calculated in order to compare with experimental and former theoretical data. Results are presented in Table 1. In addition, we obtained the bulk modulus by fitting the volume and calculated cohesive energy to Murnaghan's equation of the state. It can be seen from Table 1 that our results are in agreement with the experimental and former theoretical values.

The formation energy of intrinsic defect is given by

$$E_f = E - \frac{1}{2}(n_w + n_c)\mu_{wc} - \frac{1}{2}(n_w - n_c)(\mu_w - \mu_c), \quad (1)$$

where E is the cohesive energy of supercell with intrinsic defect, n_w and n_c are the numbers of tungsten and carbon in supercell, and μ_{wc}, μ_w and μ_c are the chemical potential of WC, tungsten and carbon, respectively. Here, μ_{wc} is taken as the cohesive energy (per formula) of WC, while μ_w and μ_c are the cohesive energy (per atom) of metallic *bcc*-W and graphite at their optimized geometries, respectively.

Table 1
The bulk properties and cohesive energy (E_c) of WC, MD and DFT mean the results obtained by molecular dynamic simulation and density functional theory, respectively.

	a_0 (nm)	c_0/a_0	B_0 (GPa)	E_c (eV)
Experiment	0.2907 [a]	0.976[a]	329[b]	−16.68[c]
MD[d]	0.2917	0.964	443	−16.68
DFT[d]	0.2979	0.975	368	−15.01
Present work	0.2932	0.973	356	−16.42

[a] Ref. [25].
[b] Ref. [26].
[c] Ref. [27].
[d] Ref. [17].

3. Results and discussion

3.1. Electronic properties

In order to investigate the influence of tungsten and carbon vacancy on the electronic structure of WC, we firstly calculate the electronic properties of perfect WC. The density of states (DOS) and valence charge density of WC are shown in Figs. 1 and 2, respectively. Here the DOS are calculated using $3 \times 3 \times 3$ supercells and $13 \times 13 \times 13$ k-grids mesh centered on the Gamma point. As can be seen from Fig. 1, the low density of electronic states at the Fermi level determines the high stability of WC, and the strongly hybridization of W-*d* and C-*p* states indicates a covalent bonding along with partially ionic W—C bonds. As shown in Fig. 2a and b, we can clearly see that there is a fairly large background charge in the basal plane, especially in the tungsten plane. From Fig. 2e the W—C nearest-neighbor bonding becomes evident. In addition to the pileup of charge in the W—C chains, there is also a delocalized component of the charge density, creating a background in the interstitial regions. Our present results are consistent with the reported results [11,13,28].

3.2. Vacancies and antisite defects

There are two types of vacancy in the WC, namely tungsten and carbon vacancy. As shown in Fig. 3, for the carbon vacancy, there are six equivalent tungsten atoms as its nearest-neighbors $\left(W_{Vc}^{N}\right)$ and the nearest-neighbor distance is 0.221 nm. In addition, there are distinct neighbor sites of carbon vacancy aligned along the ***c*** axis and in the basal plane in carbon sublattice, denoted by C_{Vc}^{c} and C_{Vc}^{b}, respectively, and their distances away from the vacancy site are 0.285 and 0.293 nm (see Fig. 3), respectively. Similar neighbors exist for tungsten vacancy, and marked with C_{Vw}^{N}, W_{Vc}^{c} and W_{Vc}^{b}. Besides, there exist two types of antisite defects that are formed by atoms located on the wrong sublattices, namely C_W and W_C, with a carbon atom on a tungsten site and a tungsten atom on carbon site,

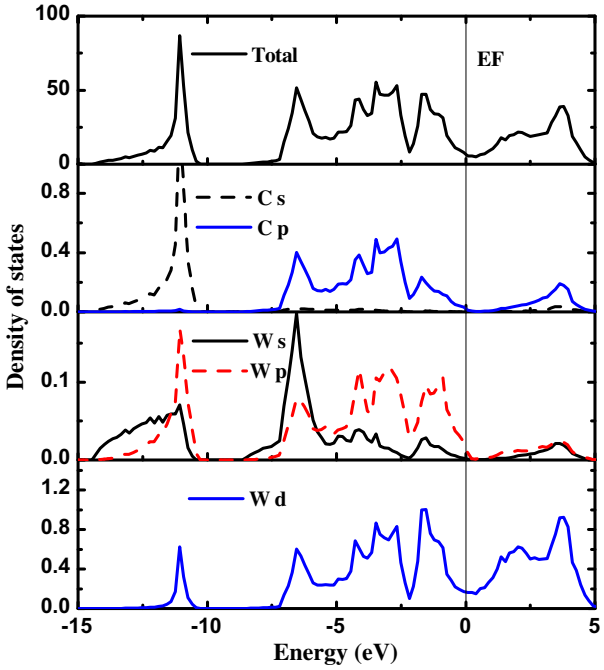

Fig. 1. The total and partial contributions to the DOS from orbital of different angular symmetry on carbon and tungsten site of WC. Zero of energy is set at the Fermi level.

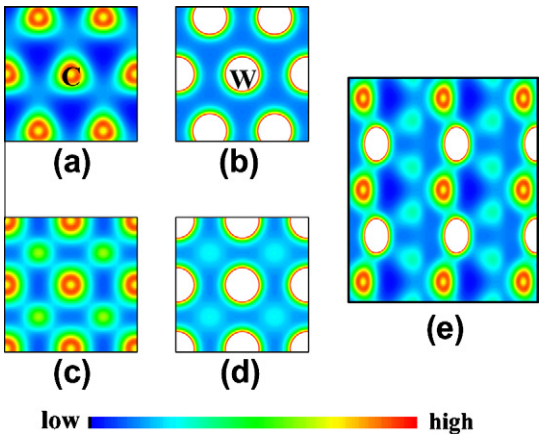

Fig. 2. The valence charge density distribution maps for WC: (a) and (b) show the valence charge density distribution for the carbon and tungsten basal plane, respectively, (c) and (d) present the valence charge density distribution for carbon and tungsten (10–10) plane, respectively and (e) are the valence charge density in (11–20) plane.

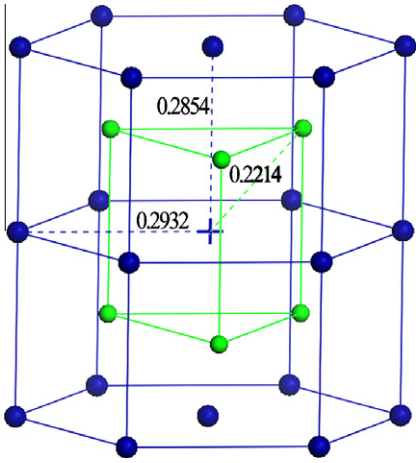

Fig. 3. The local structure of WC with a carbon vacancy. The tungsten and carbon atoms are marked in green (white) and blue (black) balls, respectively. The '+' denotes the carbon vacant site. The dash line is the distance between carbon vacant and its neighbors: 0.2214, 0.2854 and 0.2932 nm. (For interpretation of the references to colour in this figure legend, the reader is referred to the web version of this article.)

respectively. All initial defect configurations are fully relaxed to obtain the structural properties of defects and the formation energy. The formation energy is calculated using Eq. (1). In addition, the defect volume changes relative to perfect WC are calculated by

$$\Delta V/V = \frac{V_{defect} - V_0}{V_0}, \tag{2}$$

where V_{defect} and V_0 are the volume of supercell with and without defect, respectively. All related results are summarized in Tables 2 and 3.

For the vacancy defects, we find that the nearest-neighbor atoms of the vacancy relax outward, while other neighbors move inward. It is this cooperative relaxation that makes the supercell volume insensitive to the presence of vacancies at small vacancy concentration. The volume relaxations are generally small, and the defect volume changes relative to the perfect system are −0.2% and −0.4% for V_C and V_W, respectively. Similar relaxation features have been found in other transition-metal carbide [29]. The formation energy of V_C and V_W are 0.39 eV and 4.14 eV, respectively, and the later is much larger than the former. This large difference may arise from the difference in electronic properties between tungsten and carbon in WC. In the perfect WC, tungsten and carbon atoms have [WC6W8] and [CW6] coordination polyhedra, respectively. Six W—C bonds are broken to form a carbon vacancy, whereas to form a tungsten vacancy six W—C and eight W—W bonds are broken. Therefore, more energies are needed for the formation of tungsten vacancy than carbon vacancy. Our calculated results are in agreement with previous molecular dynamic calculations[17,18] but disagreement with Ivanovskii's results [15]. Note that, in Ivanovskii's study the energy of vacancy formation was estimated as a difference between the cohesive energies of stoichiometry and defect carbides and the used supercell only consist of 16 atoms, which may be one main reason of this disagreement. For the antisite defects, the formation energy of C_W and W_C are significantly larger than that of vacancy, 8.81 and 8.69 eV, respectively, suggesting that antisites are energetically less favorable. The outward relaxation around W_C is considerably large, and the defect volume change is 3.4%. It should be pointed out that the C_W is metastable. The carbon atom moves away from the tungsten vacancy site along the ***c*** direction with a barrier of 0.46 eV, and forms a relative stable defect configuration (I_C(BOC) + V_W) with the formation energy of 5.29 eV.

We examine the effect of V_C and V_W imperfections on the electronic properties of WC. Fig. 4 shows the valence charge density distribution maps for WC with a carbon or tungsten vacancy. The electron density in tungsten vacancy is much lower than that in carbon vacancy. This explains the observation of positron annihilation experiments, where the positron lifetime in carbon vacancies is considerably lower than that in W vacancies. Figs. 5 and 6 present the DOS for WC with a carbon and tungsten vacancy, respectively. Here the same supercell and *k*-grids mesh for the DOS calculation as in the defect-free case. The comparison of DOS between defective (Figs. 5 and 6) and defect-free (Fig. 1) systems shows that the introduction of a vacancy defect results in the appearance of some new peaks around the Fermi level. These peaks are generally called *vacancy peaks* in transition-metal carbides. For the carbon vacancy, these vacancy peaks are mainly of W-*d*

Table 2
$D(R)$(nm) is the distance between neighbor atom R $\left(R = W^N_{Vc}, C^c_{Vc}, C^b_{Vc}\right)$ and defect lattice site; $\Delta V/V$ (%) is defect volume changes relative to the perfect system; E_f (eV) is the formation energy of defect in configuration; E_F (eV) is the Fermi energy; $N(E_F)$ is the DOS on the Fermi level.

	Perfect	V_C	W_C
$D\left(W^N_{Vc}\right)$	0.2214	0.2231	0.2454
$D(C^c_{Vc})$	0.2854	0.2842	0.2817
$D\left(C^b_{Vc}\right)$	0.2932	0.2908	0.3023
$\Delta V/V$		−0.2	3.4
E_f		0.39	8.69
E_F	7.77	7.64	7.44
$N(E_F)$	5.574	7.509	12.96

Table 3
$D(R)$(nm) is the distance between neighbor atom R $\left(R = C^N_{Vw}, W^c_{Vc}, W^b_{Vc}\right)$ and defect lattice site; $\Delta V/V$ (%) is defect volume changes relative to the perfect system; E_f (eV) is the formation energy of configuration.

	Perfect	V_W	C_W
$D\left(C^N_{Vw}\right)$	0.2214	0.2311	0.2330
$D(W^c_{Vc})$	0.2854	0.2762	0.2809
$D\left(W^b_{Vc}\right)$	0.2932	0.2900	0.2911
$\Delta V/V$		−0.4	−0.1
E_f		4.14	8.81

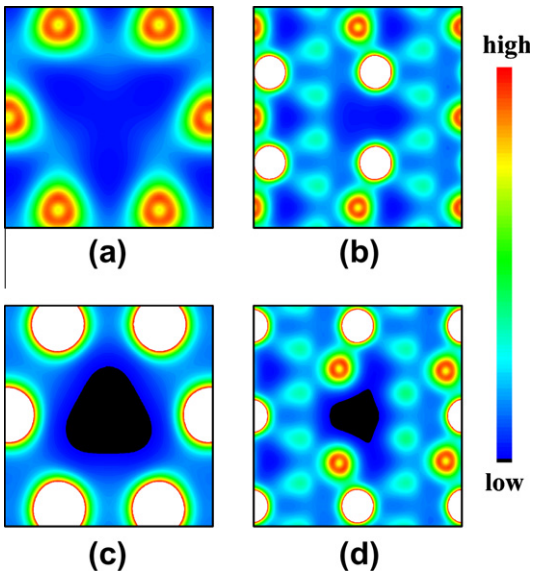

Fig. 4. The valence charge density distribution maps for WC with vacancy defect: (a) and (b) are the valence charge density of WC with carbon vacancy in the carbon basal plane and the (11–2 0) plane, respectively; (c) and (d) are the valence charge density of WC with tungsten vacancy in the tungsten basal plane and the (11–2 0) plane, respectively.

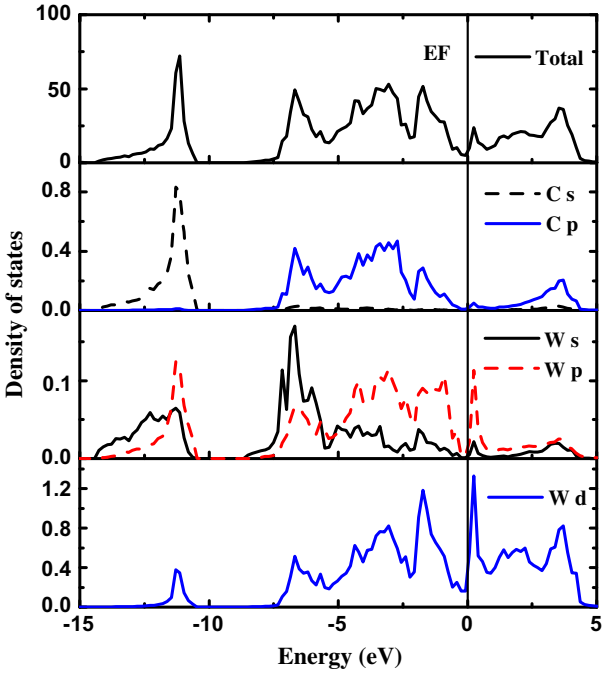

Fig. 5. Density of states for WC with a carbon vacancy.

character. While the effect of tungsten vacancy on the spectrum of WC not only depends on the change in the electronic states of carbon atoms nearest to the vacancy, but also relates to that of tungsten atoms surrounding the vacancy. These peaks are similar to that reported previously [16]. The origin of these peaks is possible to explain as that the emptying of a part of bonding states takes place in the presence of both carbon and tungsten vacancy. In addition, the Fermi level (E_F) is shifted to the lower energy range and the DOS on the Fermi level ($N(E_F)$) increase after introduction of vacancies (Table 2). This impairs the cohesive properties of WC and decreases the stability of system. Note that the density of

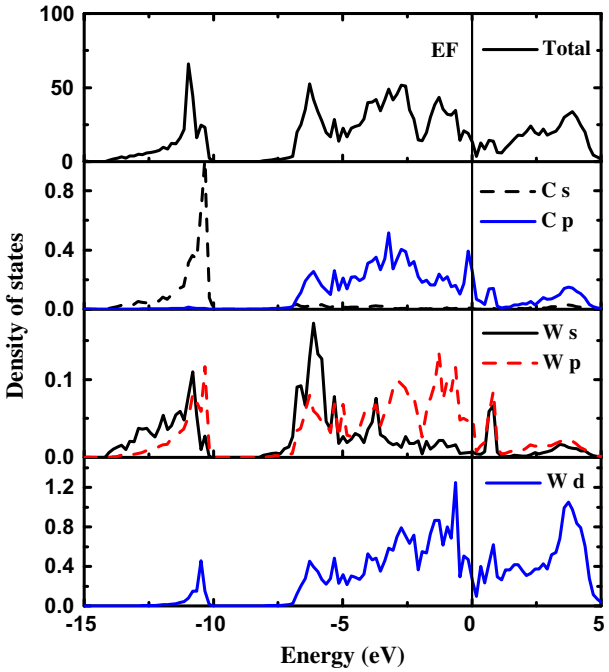

Fig. 6. Density of states for WC with a tungsten vacancy.

states at the Fermi level for tungsten vacancy increase more rapidly. This results in lower cohesive properties as compared with carbon vacancy.

3.3. Self-interstitial defect

In WC, there are eighteen possible interstitial configurations as shown in Figs. 7 and 8. Fig. 7 shows the ten different interstitial sites. In naming the interstitial sites, we have adopted a similar notation system to those used in pure metal with *hcp* structure [30]. O is the octahedral interstitial sites formed by equivalent three tungsten atoms and three carbon atoms. BOC and BOW are

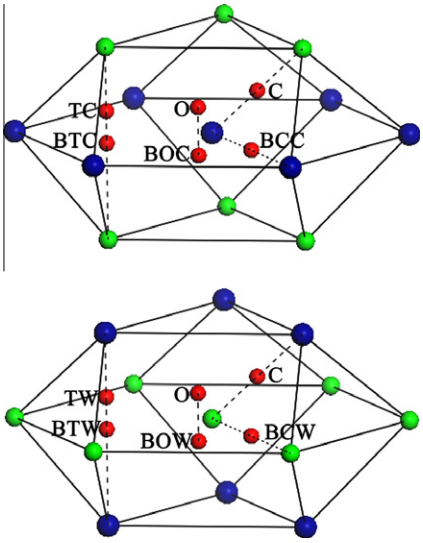

Fig. 7. Schematic diagram of various isolated interstitial sites in WC. The tungsten and carbon atoms are marked in green (white) and blue (black) balls, respectively. The smaller red (dark gray) balls represent the interstitial sites. (For interpretation of the references to colour in this figure legend, the reader is referred to the web version of this article.)

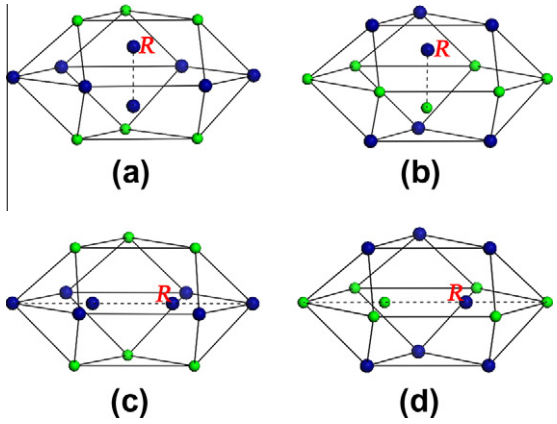

Fig. 8. Schematic diagram of four carbon split-interstitial configurations in WC. The tungsten and carbon atoms are marked in green (white) and blue (black) balls, respectively. For tungsten split-interstitial configurations, the carbon atom denoted by red *R* would be replaced by tungsten atom. (For interpretation of the references to colour in this figure legend, the reader is referred to the web version of this article.)

carbon and tungsten basal plane projection of O site, respectively. There exist two different tetrahedral interstitial sites, i.e., TC and TW, which are formed by two different atomic clusters: the former is composed of three carbon atoms and one tungsten atom and the later consists of three tungsten atoms and one carbon atom. Similarly, BTC and BTW are hexahedral sites formed by two different atomic clusters: the former is formed by three carbon atoms and two tungsten atoms, while the later is made up of three tungsten atoms and two carbon atoms. C is the midway between the nearest-neighbor tungsten and carbon atom. BCC/BCW is the midway between two nearest carbon/tungsten atoms in the dense **a** direction in carbon/tungsten basal plane. Fig. 8 shows four possible carbon split-interstitial configurations, which are denoted by the symbols SCC, SWC, BSCC, and BSWC, and described as follows: SCC (Fig. 8a), two carbon atoms are symmetrically split in the ***c*** direction about a carbon vacant normal lattice site; SWC (Fig. 8b), a tungsten atom shares a tungsten vacant normal lattice site with a carbon atom in the ***c*** direction; BSCC (Fig. 8c), two carbon atoms are symmetrically split in the dense ***a*** direction about a carbon vacant normal lattice site; BSWC (Fig. 8d), a tungsten atom shares a tungsten vacant normal lattice site with a carbon atom in the dense ***a*** direction. Similar configurations exist for tungsten split interstitials. They are named by SCW, SWW, BSCW, and BSWC, respectively. Note that, the pairs of atoms are approximately 1/2 c_0 and 2/3 a_0 apart in the split-interstitial configuration along the ***c*** and dense ***a*** direction, respectively.

These interstitial configurations are fully relaxed, and the formation energies of stable configurations are calculated using Eq. (1). In addition, we also calculate the defect volume changes relative to perfect WC using Eq. (2). These results are summarized in Tables 4 and 5. For carbon interstitial, we identified a C—C dimer configuration (***a***-dimer) relaxed from the BSCC as the lowest energy state. This dimer along the ***a*** direction and its bond length is 0.131 nm. The formation energy of ***a***-dimer configurations is 3.14 eV. It should be noted that the center of ***a***-dimer has shifted away the carbon vacant site as shown in Fig. 9. We find five metastable carbon interstitial configurations, i.e., BOC, ***c***-dimer, BTW, BOW, and BTC. In the ***c***-dimer configuration, two carbon atoms share a carbon vacant site along the ***c*** direction. For tungsten interstitial, the most stable configuration is BOC with a formation energy of 11.51 eV. Two complex-defects are also found, namely I_C(BOC) + W_C (Fig. 9b) and I_C(BTW) + W_C (Fig. 9d), consisting of an interstitial carbon defect and a W_C antisite defect, which have a

Table 4
Calculation results for carbon and tungsten self-interstitial defects in WC. $\Delta V/V$ (%) is defect volume changes relative to the perfect system; E_f (eV) is the formation energy of defect configuration.

	Carbon interstitial defect			Tungsten interstitial defect		
	Final configuration	E_f	$\Delta V/V$	Final configuration	E_f	$\Delta V/V$
O	BOC	3.41	0.75	BOC	11.58	4.67
BOC	BOC	3.41	0.75	BOC	11.58	4.67
BOW	BOW	5.00	1.82	BOW	13.48	4.94
C	BOC	3.41	0.75	I_C(BOC) + W_C	9.73	3.80
BCC	BOC	3.41	0.75	BOC	11.58	4.67
BCW	BTW	4.37	1.96	*c*-Crowdion	13.65	5.32
TC	BTC	5.63	1.74	*a*-Crowdion	15.62	5.00
BTC	BTC	5.63	1.74	*a*-Crowdion	15.62	5.00
TW	BTW	4.37	1.96	I_C(BTW) + W_C	10.65	5.21
BTW	BTW	4.37	1.96	BTW	15.96	5.94

Table 5
Formation energy of final defect configurations obtained from the relaxation of split-interstitial configurations. $\Delta V/V$ (%) is defect volume changes relative to the perfect system; E_f (eV) is the formation energy of defect configuration.

	Final configuration	E_f	$\Delta V/V$
SCC	*c*-Dimer	3.53	2.08
SWC	I_C(BTC)	5.63	1.74
BSCC	*a*-Dimer	3.14	1.64
BSWC	I_C(BTW)	4.37	1.96
SCW	I_C(BTW) + W_C	10.69	5.21
SWW	*c*-Crowdion	15.62	5.00
BSCW	I_C(BOC) + W_C	9.73	3.80
BSWW	*a*-Crowdion	13.76	5.32

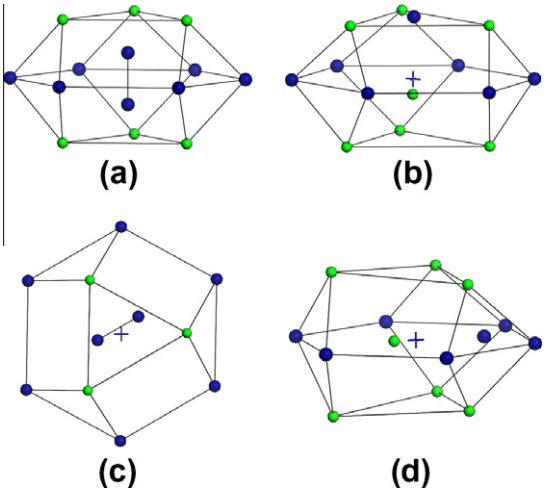

Fig. 9. Schematic diagram of final configurations in WC with a interstitial carbon or tungsten atom. The tungsten and carbon atoms are marked in green (white) and blue (black) balls, respectively. The '+' denotes the carbon vacant site. (For interpretation of the references to colour in this figure legend, the reader is referred to the web version of this article.)

little lower formation energy than interstitial tungsten defects. This indicates that the tungsten will occupy the lattice site when a tungsten atom and a carbon atom share a vacant site. We also observe two crowdion defects along the ***a*** and ***c*** direction, respectively. Their formation energies are considerably high, about 13.65 and 15.62 eV, respectively. In a word, the defect formation energies of tungsten interstitial are considerably high. This means that interstitial tungsten defects are energetically much less favorable. Therefore, under normal conditions, WC has no tungsten interstitial defects [31]. Comparing with the case of carbon

interstitial, the defect volume changes of all tungsten interstitial configurations are much larger. The key to understanding the large difference in the formation energy between tungsten and carbon defects lies in the covalent property of W—C bond and the large mismatch in the covalent radii of tungsten (r_W = 0.130 nm) and carbon (r_W = 0.077 nm). As an example we investigate the influence of this mismatch on defect formation energies of the tungsten antisite defect based on data of Table 2. When a carbon atom is replaced by a tungsten atom, the W—C bonds are replaced by W—W bonds. Without atomic relaxation the W—W bonds are 18.4% smaller than W—W bonds in pure tungsten bulk. If atomic relaxation is allowed, the six neighboring tungsten atoms move outward about 0.022 nm, reducing the strain in the W—W bond. The atomic relaxation is accompanied by an energy gain. However, even large energy gain due to relaxation can not avoid that the tungsten antisite remains energetically unfavorable. The large energy gain is only a response to the huge internal strain which is built up by forming this antisite. Atomic relaxation can reduce this strain; however, it can not completely avoid it. The same argumentation applies for the tungsten interstitial.

3.4. Diffusion properties

Based on the above optimized geometry of defects, we investigate the diffusion properties of the stable intrinsic defects in WC. It should be pointed out that here we have not considered the diffusion properties of those defects which are thermodynamically unlikely but could easily be formed during collision events under irradiation. We firstly study the carbon vacancy diffusion property in WC. In the WC, there are distinct sites aligned along the ***c*** axis and in the basal plane. Hence, there are two possible transition paths for carbon vacancy: one path propagates parallel to the ***c*** axis and the other path is the diffusion of carbon vacancy in the basal plane. The former is denoted as PC_V, and the latter is marked by PB_V. We calculate the transition states and barrier energies of these two pathes using the NEB method. The saddle-point structure of PC_V is that the carbon atom is equidistant from two vacant carbon lattice site in the ***c*** direction, i.e., BTW interstitial site (Fig. 10a), while that of PB_V is that the carbon atom locates the BOC as shown in Fig. 10b. The energy barrier of PC_V and PB_V are 6.59 and 3.28 eV, respectively. The former are much higher than the later, showing that carbon vacancies prefers to diffusion in the basal plane. Schematic representations of these diffusion paths are shown in Fig. 10. The feature of high vacancy diffusion barriers together with the low formation energy of carbon vacancy and the high formation energy of tungsten interstitial is very important on the stability of substoichiometric (WC_x with $x < 1$) case. It implies that once substoichiometric WC are formed, the lattice stays intact because carbon vacancies do not hop to other sites, unless the system are annealed at very high temperatures and for long periods of time. It should be pointed out that the migration barrier of 3.3 eV for carbon vacancy is a little large to explain the experimental observed annealing stage at 800 K [14], and it needs to be further studied.

We now investigate migration of interstitial carbon atom. As it has been discussed above, there are many metastable interstitial configurations, which would transform into more stable configurations. According to the above calculated results, we find that the most stable configuration for carbon interstitial is ***a***-dimer configuration, followed by the BOC configuration. Hence, we investigate the transformation of BOC into ***a***-dimer configuration, which are shown in Fig. 11. The barrier energy of the transformation of BOC into ***a***-dimer configuration is 0.32 eV. This lower activation energy evinces that carbon interstitial migration is activated at lower temperatures. In addition, we also calculated the diffusion of interstitial carbon atom along the ***c*** direction. Its barrier energy is 2.20 eV (Fig. 11), which is much higher than that of the diffusion in carbon basal plane. This implies that the interstitial carbon atom prefers to diffusion in the carbon basal plane.

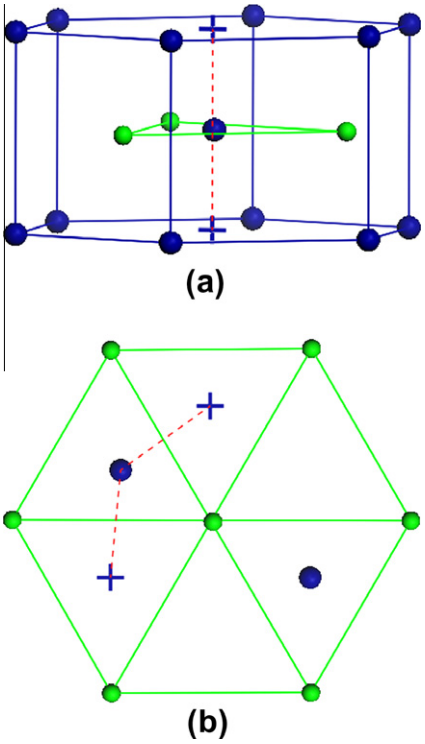

Fig. 10. Schematic of the mechanism for carbon vacancy in WC: (a) and (b) show diffusion paths PC_V and PB_V, respectively. The '+' denoted the initial and final vacancy site. The red dash lines are guides to the eyes for these diffusion paths. The blue and green balls are the tungsten and carbon atoms, respectively, in the saddle-point structure. (For interpretation of the references to colour in this figure legend, the reader is referred to the web version of this article.)

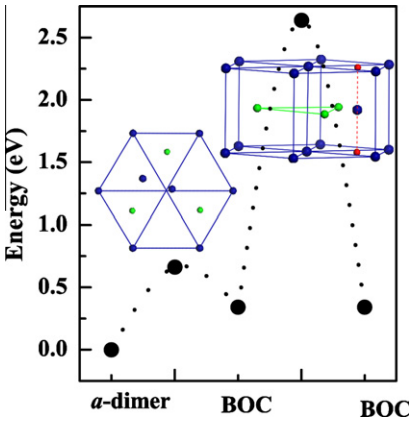

Fig. 11. Energy barrier for the migration of interstitial carbon atom. The tungsten and carbon atoms are marked in green (white) and blue (black) balls. The small red balls are the initial and final interstitial sites BOC. The red dash lines are guides to the eyes for the diffusion path. (For interpretation of the references to colour in this figure legend, the reader is referred to the web version of this article.)

4. Conclusion

We use first-principles calculations to study the stability of point defects and their complexes in WC. Our calculation results confirm that the formation energies of carbon defects are much lower than that of tungsten defects. Comparing with other intrinsic

defects, the carbon vacancy has a much smaller formation energy and higher diffusion barrier. This implies that the carbon vacancy is the dominant defects in WC. The C—C dimer configurations along the dense ***a*** direction is the most stable configuration of carbon interstitial defect. For interstitial tungsten atom, the preferentially occupation site is BOC. In addition, the tungsten will occupy the lattice site when a tungsten atom and a carbon atom share a vacant site. We have firstly investigated the atomic-scale mechanism of carbon defect diffusion in WC. The results show that the carbon vacancies stay for a wide range of temperature because of extremely high diffusion barriers, while carbon interstitial migration is activated at lower temperatures for its considerably lower activation energy. Both of them prefer to diffusion in carbon basal plane.

Acknowledgement

This work was supported by the National Magnetic Confinement Fusion Program (Grant No. 2009GB106005) and the Innovation Program of Chinese Academy of Sciences (Grant No. KJCX2-YW-N35), and by the Center for Computation Science, Hefei Institutes of Physical Sciences.

References

[1] M. Kaufmann, R. Neu, Fus. Eng. Des. 82 (2007) 521.
[2] J. Pamela, G.F. Matthews, V. Philipps, R. Kamendje, J. Nucl. Mater. 363C365 (2007) 1.
[3] R.P. Doerner, J. Nucl. Mater. 363C365 (2007) 32.
[4] W. Eckstein, J. Roth, Nucl. Instrum. Meth. B 53 (1991) 279.
[5] H. Kimura, Y. Nishikawa, T. Nakahata, M. Oyaidzu, Y. Oyab, K. Okunoa, Fus. Eng. Des. 81 (2006) 295.
[6] K. Sugiyama, K. Krieger, C.P. Lungu, J. Roth, J. Nucl. Mater. 390C391 (2009) 659.
[7] K.A. Beadle, R. Gupta, A. Mathew, J.G. Chen, B.G. Willis, Thin Solid Films 516 (2008) 3847.
[8] H.W. Hugosson, H. Engqvist, Int. J. Ref. Met. Hard Mater. 21 (2003) 55.
[9] E.I. Isaev, S.I. Simak, I.A. Abrikosov, R. Ahuja, Yu.Kh. Vekilov, M.I. Katsnelson, A.I. Lichtenstein, B. Johansson, J. Appl. Phys. 101 (2007) 123519.
[10] L.F. Mattheiss, D.R. Hamann, Phys. Rev. B 30 (1984) 1731.
[11] A.Y. Liu, R.M. Wentzcovitsh, M.L. Cohen, Phys. Rev. B 38 (1988) 9483.
[12] D.L. Price, B.R. Cooper, Phys. Rev. B 39 (1989) 4945.
[13] D.V. Suetin, I.R. Shein, A.L. Ivanovskii, J. Phys. Chem. Solid 70 (2009) 64.
[14] A.A. Rempel, R. Wurschum, H.E. Schaefer, Phys. Rev. B 61 (9) (2000) 5945.
[15] A.L. Ivanovskii, N.I. Medvedeva, Mendeleev Commun. 1 (2001) 10.
[16] N.I. Medvedeva, A.L. Ivanovskii, Phys. Solid State 43 (2001) 469.
[17] N. Juslin, P. Erhart, P. Träkelin, J. Nord, K.O.E. Henriksson, K. Nordlund, E. Salonen, K. Albe, J. Appl. Phys. 98 (2005) 123520.
[18] C. Björkas, K. Vötler, K. Nordlund, Phys. Rev. B 74 (2006) 140103.
[19] G. Kresse, J. Hafner, Phys. Rev. B 47 (1993) 558.
[20] G. Kresse, J. Furthmüler, Phys. Rev. B 54 (1996) 11169.
[21] G. Kresse, D. Joubert, Phys. Rev. B 59 (1999) 1758.
[22] P.E. Blöchl, Phys. Rev. B 50 (1994) 17953.
[23] J.P. Perdew, J.A. Chevary, S.H. Vosko, K.A. Jackson, M.R. Pederson, D.J. Singh, C. Fiolhais, Phys. Rev. B 46 (1992) 6671;
J.P. Perdew, J.A. Chevary, S.H. Vosko, K.A. Jackson, M.R. Pederson, D.J. Singh, C. Fiolhais, Phys. Rev. B 48 (1993) 4978(E).
[24] H.J. Monkhorst, J.D. Pack, Phys. Rev. B 13 (1976) 5188.
[25] H.O. Pierson, Handbook of Refractory Carbides and Nitrides: Properties Characteristics, Processing, and Applications Noyes, Westwood, NJ, 1996.
[26] H. L Brown, P.E. Armstrong, C.P. Kempter, J. Chem. Phys. 45 (1966) 547.
[27] D.R. Lide (Ed.), CRC Handbook of Chemistry and Physics, 85th ed., CRC, Boca Raton, 2004.
[28] N. Gaston, S. Hendy, Catal. Today 146 (2009) 223.
[29] L. Tsetseris, S.T. Pantelides, Acta Mater. 56 (2008) 2864.
[30] F. Willaime, J. Nucl. Mater. 323 (2003) 205.
[31] A.S. Kurlov, A.I. Gusev, Russ. Chem. Rev. 75 (7) (2006) 617.